Angewandte Chemie
Eine Zeitschrift der Gesellschaft Deutscher Chemiker

Supporting Information

69451 Weinheim, Germany

Uncovering the Stoichiometry of *Pyrococcus furiosus* RNase P, a Multi-Subunit Catalytic Ribonucleoprotein Complex, by Surface-Induced Dissociation and Ion Mobility Mass Spectrometry**

Xin Ma, Lien B. Lai, Stella M. Lai, Akiko Tanimoto, Mark P. Foster, Vicki H. Wysocki, and Venkat Gopalan**

anie_201405362_sm_miscellaneous_information.pdf

Abbreviations used

MS, mass spectrometry; MS/MS, tandem MS; IM, ion mobility; SID, surface-induced dissociation; CID, collision-induced dissociation; RPR, RNase P RNA; RPP, RNase P Protein; pre-tRNA, precursor tRNA

Experimental

MS/MS and IM-MS

IM-MS was performed on a Synapt G2 HDMS (Waters MS Technologies, Manchester, UK)[1] modified to include a customized SID device[2] before the IM cell to record the drift time of the SID fragments.

For nano-electrospray ionization, each sample was loaded into a tapered glass capillary (inner diameter of the non-tapered end was 1 mm) pulled in-house using a Sutter Instruments P-97 micropipette puller (Novato, CA). A platinum wire was inserted into the non-tapered end of the capillary, and a voltage of 1.4-1.7 kV was applied. The cone voltage was empirically optimized at 50 V for binary RPPs and 200 V for RNP complexes. The ion source temperature was kept at ~30°C to minimize denaturation of RPPs. Pressure in the source region was raised to ~6 mbar by partially restricting the vacuum line to the rotary pump to optimize ion collisional cooling and transmission. For SID experiments, ions were accelerated by increasing "trap DC bias" and steered toward a fluorinated hydrocarbon ($CF_3(CF_2)_9CH_2CH_2S$)-coated gold surface by manipulating the lens voltages in the device. When collecting MS and CID spectra, the voltages of the SID device were set to ensure that the ions passed through the cells without hitting the surface. Collision-induced cleaning and CID were performed in the trap cell, the first ion guide collision cell in the instrument.

All samples were analyzed with argon as the collision gas and nitrogen as the ion mobility gas. The pressure of argon in the transfer ion guide was ~3×10^{-2} mbar, while the pressure in the trap was either 3.3×10^{-2} mbar for RPP complexes and SID experiments or 6×10^{-2} mbar for MS and CID MS/MS of RNP complexes; the 6×10^{-2} mbar pressure selectively and effectively transmits high *m/z* ions. In MS experiments, trap collision energy ("Trap CE") was set at 4 V for binary RPPs, but was increased to 15 V for improved transmission of RNP complexes.

CID MS/MS was performed over a range of collision voltages from 30 V to 200 V in the trap collision cell. The flow rate to the helium cell, which was used for collisional cooling at the entrance of the IM chamber,[1b] was 120 mL/min. The pressure of nitrogen in the ion mobility cell was 2.2 mbar. The IM-MS wave height and velocity were optimized at 20 V and 200 m/s, respectively. The pressure in the time-of-flight (TOF) analyzer was $0.7\text{-}1\times10^{-6}$ mbar. The IM-MS conditions were optimized based on earlier reports.[3]

Over-expression and purification of Pfu RPP21•RPP29 and POP5•RPP30

Co-overexpression in *Escherichia coli* BL21(DE3) cells and subsequent purification of *Pfu* binary RPP complexes (RPP21•RPP29 and POP5•RPP30) were performed as described previously.[4] The purified RPP complexes were dialyzed against storage buffer [50 mM HEPES-KOH, pH 8; 800 mM NH_4OAc; 6 mM $MgCl_2$] and stored at 25°C until further use.

In vitro transcription of Pfu RPR and pre-tRNA^{Tyr}

Pfu RPR *and* pre-tRNA^{Tyr} were generated by T7 RNA polymerase-mediated run-off transcription using previous protocols.[4-5] The resultant RNA transcripts were subsequently extracted with phenol-chloroform, dialyzed extensively against water (using a 3.5-kDa molecular weight cut-off membrane) to remove unincorporated nucleotide triphosphates, precipitated, and quantitated based on absorbance at 260 nm and their respective extinction coefficients.

Sample preparation for native MS

Purified recombinant binary RPP complexes were dialyzed for 16 h at 25°C against 10 mM NH_4OAc in Slide-A-Lyzer MINI dialysis units (10-kDa molecular weight cut-off; Pierce, Rockford, IL). *Pfu* RPR folding entailed incubating 100 μM *in vitro* transcribed RPR in water for 50 min at 50°C and 10 min at 37°C before adding an equal volume of 2X folding buffer [1.6 M NH_4OAc; 20 mM $Mg(OAc)_2$]; the resulting 50 μM RPR sample was then incubated for an additional 30 min at 37°C. MS samples were prepared by mixing *Pfu* RPR and RPPs (final concentration = 5 μM of each subunit) with NH_4OAc and $Mg(OAc)_2$ (as specified) and incubating for 10-20 min at 55°C.

In addition to RPP21•RPP29 and POP5•RPP30, the ribosomal protein L7Ae has been shown to act as a fifth archaeal RPP.[6] We are now investigating the contribution of *Pfu* L7Ae to RNase P activity *in vitro*, but have yet to determine the optimal conditions for its participation in RNase P assembly and function. In the absence of such biochemical characterization, MS experiments with L7Ae could not be included in the present studies.

RNase P activity assays

Pre-tRNA processing assays were conducted in parallel in both MS buffer and *Pfu* RNase P assay (PRA) buffer. *Pfu* RPR was folded largely as described for the MS experiments. One hundred μM *in vitro* transcribed *Pfu* RPR in water was incubated for 50 min at 50°C and 10 min at 37°C before adding an equal volume of 2X folding buffer – either MS [1.6 M NH_4OAc; 20 mM $Mg(OAc)_2$] or PRA [100 mM HEPES-KOH, pH 8; 1.6 M NH_4OAc; 20 mM $MgCl_2$]. After addition of the respective buffer, the RPR was incubated for an additional 30 min at 37°C. RPPs dialyzed against 10 mM NH_4OAc were used for the RNase P assays in MS buffer, while those dialyzed against storage buffer were used for the reactions in PRA buffer. To assemble the *Pfu* RNase P complex, 5 μM folded RPR (final) was pre-incubated with 5 μM RPPs in MS buffer [800 mM NH_4OAc; 2 or 3 mM $Mg(OAc)_2$] or PRA buffer [50 mM HEPES-KOH, pH 8; 800 mM NH_4OAc; 2 or 3 mM $MgCl_2$] for 10 min at 55°C. A trace amount (4,000 dpm) of *E. coli* pre-$tRNA^{Tyr}$, 5′-labeled with ^{32}P, was added to each single-turnover reaction in which the enzyme was in vast excess over the substrate (at least 1000-fold). After incubation for 30 min at 55°C, the reactions were quenched with two volumes of urea dye [7 M urea; 1 mM EDTA; 0.05% (w/v) xylene cyanol; 0.05% (w/v) bromophenol blue; 10% (v/v) phenol]. Substrate control reactions (i.e., in the absence of enzyme) in each buffer were also prepared and incubated in parallel with its corresponding assay reaction. The reaction products were separated using an 8% (w/v) polyacrylamide/8 M urea gel, visualized using a Typhoon (GE Healthcare) phosphorimager, and the final figure arranged and annotated in Adobe Photoshop (Adobe Systems).

Acknowledgements

We are extremely grateful to Royston Quintyn, Yang Song and Andrew van Schoiack (OSU) for their kind assistance with simulating the spectra for the RPR in the absence and presence of POP5•RPP30.

References

[1] a) K. Giles, S. D. Pringle, K. R. Worthington, D. Little, J. L. Wildgoose, R. H. Bateman, Rapid Commun. Mass Spectrom. 2004, 18, 2401-2414; b) K. Giles, J. P. Williams, I. Campuzano, Rapid Commun. Mass Spectrom. 2011, 25, 1559-1566.

[2] M. Zhou, S. Dagan, V. H. Wysocki, Angew. Chem. Int. Ed. Engl. 2012, 51, 4336-4339; Angew. Chem. 2012, 124, 4412-4415.

[3] a) B. T. Ruotolo, J. L. P. Benesch, A. M. Sandercock, S.-J. Hyung, C. V. Robinson, Nat. Protoc. 2008, 3, 1139-1152; b) Y. Zhong, S.-J. Hyung, B. T. Ruotolo, Analyst 2011, 136, 3534-3541; c) C. Atmanene, S. Petiot-Becard, D. Zeyer, A. Van Dorsselaer, V. Vivat Hannah, S. Sanglier-Cianferani, Anal. Chem. 2012, 84, 4703-4710.

[4] W.-Y. Chen, D. K. Pulukkunat, I.-M. Cho, H.-Y. Tsai, V. Gopalan, Nucleic Acids Res. 2010, 38, 8316-8327.

[5] H.-Y. Tsai, D. K. Pulukkunat, W. K. Woznick, V. Gopalan, Proc. Natl. Acad. Sci. U.S.A. 2006, 103, 16147-16152.

[6] a) I.-M. Cho, L. B. Lai, D. Susanti, B. Mukhopadhyay, V. Gopalan, Proc. Natl. Acad. Sci. U.S.A. 2010, 107, 14573-14578; b) H. Fukuhara, M. Kifusa, M. Watanabe, A. Terada, T. Honda, T. Numata, Y. Kakuta, M. Kimura, Biochem. Biophys. Res. Commun. 2006, 343, 956-964.

[7] a) A. L. Feig, O. C. Uhlenbeck in The RNA World, 2nd edition (Eds.: R. F. Gesteland, T. R. Cech, J. F. Atkins), CSH Laboratory Press, Cold Spring Harbor, NY, 1999, pp. 287-319; b) J. C. Kurz, C. A. Fierke, Biochemistry 2002, 41, 9545-9558.

[8] a) T. Honda, Y. Kakuta, K. Kimura, J. Saho, M. Kimura, J. Mol. Biol. 2008, 384, 652-662; b) S. Kawano, T. Nakashima, Y. Kakuta, I. Tanaka, M. Kimura, J. Mol. Biol. 2006, 357, 583-591; c) Y. Xu, C. D. Amero, D. K. Pulukkunat, V. Gopalan, M. P. Foster, J. Mol. Biol. 2009, 393, 1043-1055.

Table S-1
Predicted and observed masses of *Pfu* RNase P subunits and complexes

Species	Predicted mass, Da	Observed mass, Da	Standard deviation, Da	Mass difference, Da	Mg^{2+} concentration
RPP21	14,172	14,203	36	31	-
RPP29	14,953	14,959	13	6	-
POP5	13,708	13,710	5	2	-
RPP30	24,363	24,367	8	4	-
RPP21•RPP29	29,125	29,502	61	377	-
$(POP5•RPP30)_2$	76,142	77,220	461	1,078	-
RPR	110,192	111,900	810	1,708	2 mM
RPR+POP5•RPP30	148,263	Overlap	NA	NA	6 mM
RPR+RPP21•RPP29	139,317	142,045	613	2,728	10 mM
$RPR+(POP5•RPP30)_2$	186,334	188,292	130	1,958	4 mM
RPR+POP5•RPP30+RPP21•RPP29	177,388	179,870	143	2,482	2 mM

Means and standard deviations calculated from three or more independent measurements. Observed masses for RPP monomeric species are from MS/MS of the corresponding binary RPP in Figure 1. The observed masses of RPR and RNP complexes are up to 2,728 Da larger than the theoretical masses, likely due to non-specific association with Mg^{2+}, ammonium acetate, and water. The electrostatic attraction of ions to polyelectrolytes like RNAs is well documented, and values ranging from 0.3 to 0.7 Mg^{2+}/nucleotide in different RNAs (including a bacterial RPR) have been reported.[7] Our use of collision-induced cleaning for improving peak resolution likely contributed to a lower and variable Mg^{2+}/nucleotide ratio than those reported previously for other RNAs. NA, not applicable; peak overlap with the RPR prevented accurate centroid assignment of adducted species.

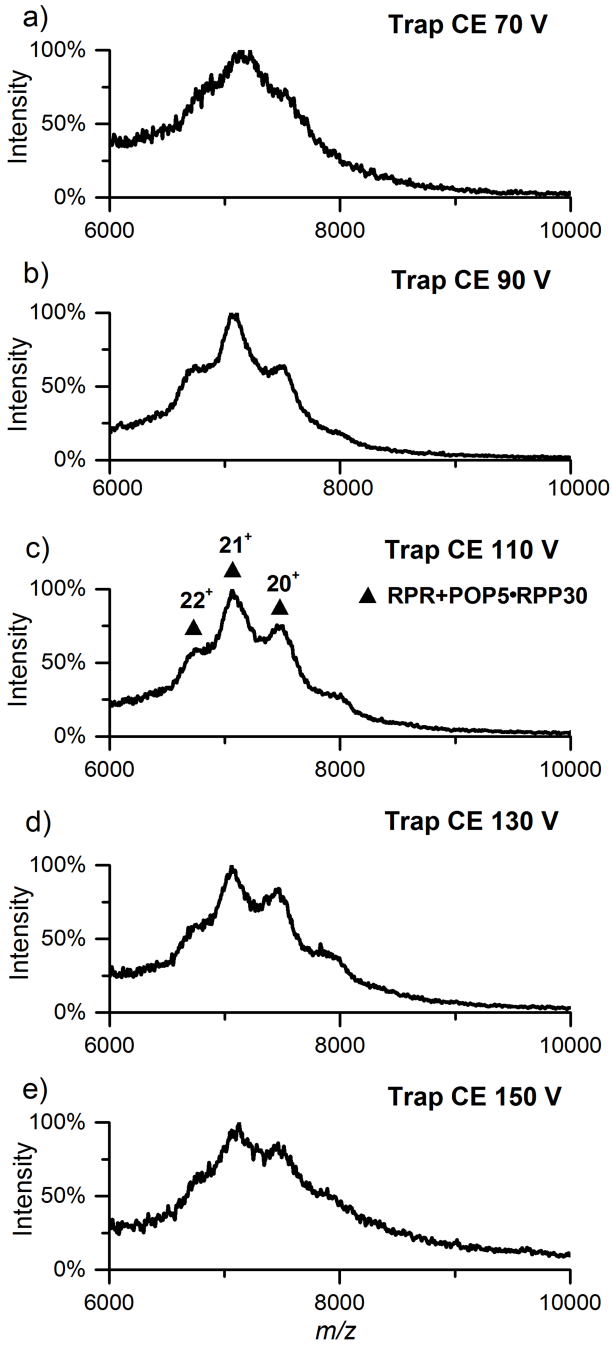

Figure S-1. Trap CE optimization of RPR and POP5•RPP30 assembled in 500 mM NH_4OAc and 6 mM $Mg(OAc)_2$. While peak broadening is evident at both low and high trap CE, resolved peaks are observable in a narrow trap CE range.

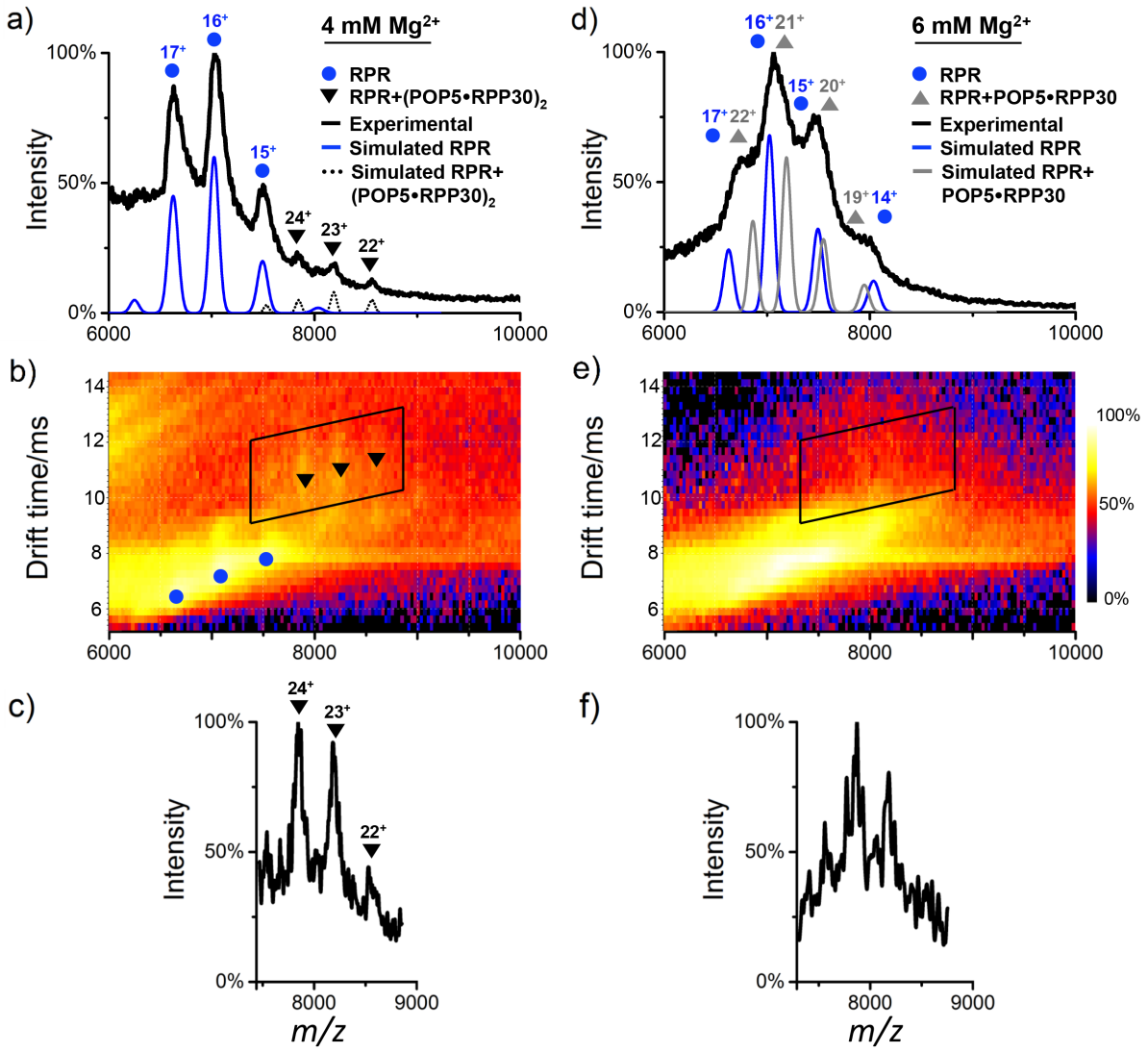

Figure S-2. Analysis of RPR assembled with POP5•RPP30 in 500 mM NH_4OAc and either 4 mM (a-c) or 6 mM $Mg(OAc)_2$ (d-f). (a) The IM-MS spectrum of RPR assembled with POP5•RPP30 at 4 mM $Mg(OAc)_2$ (with trap CE at 70 V) and (b) the corresponding mobiligram (drift time versus m/z; shown in log scale). The drift times of the higher *m/z* peaks [RPR+$(POP5•RPP30)_2$] are longer, and the peaks are marked with a black box. c) The extracted mass spectrum from the black box in (b) clearly identifies RPR+$(POP5•RPP30)_2$ peaks. (d) The IM-MS spectrum of RPR assembled with POP5•RPP30 at 6 mM $Mg(OAc)_2$ (with trap CE at 110 V) and (e) the corresponding mobiligram. The intensity of the peaks corresponding to the RPR+$(POP5•RPP30)_2$ has decreased significantly (see region marked with a black box). f) The extracted mass spectrum from the black box in (e) does not yield peaks that can be assigned with confidence, although there is similarity to the spectrum extracted and shown in (c) but with poorer signal/noise ratio, suggesting a significantly reduced abundance of

RPR+(POP5•RPP30)$_2$.

In (a) and (d), simulated Gaussians curves are used to indicate RPR (blue line; adduct mass ~2300 based on experimental peak positions), RPR+(POP5•RPP30)$_2$ (black dashed line, adduct mass ~2000 based on experimental peak position), RPR+POP5•RPP30 (gray line, ~2700 adduct mass was used based on that observed with RPR+RPP21•RPP29). The RPR and RPR+(POP5•RPP30)$_2$ peak positions are clear from figure (a), while the RPR+POP5•RPP30 in (d) is supported by the fact that its inclusion provides a better fit to the observed data than RPR alone. Note that RPR and RPR+POP5•RPP30 are not separated in drift time (panel e), suggesting similar cross sections for RPR and RPR+POP5•RPP30, with measurably different drift times for RPR and RPR+(POP5•RPP30)$_2$.

The simulations of RPR, RPR+POP5•RPP30, and RPR+(POP5•RPP30)$_2$ were generated based on the empirical peaks calculated using the Gaussian function below.

$$f(x) = Y \exp\left(-\frac{(x-\mu)^2}{2\sigma^2}\right)$$

Independent Gaussian curves for each charge state were determined based on this function, where Y = peak height, x = *m/z*, μ = position of the center of the Gaussian curve, and σ = peak width/6. Y was obtained after baseline correction. Values of x sampled for simulation were based on the experimental *m/z* range. μ is the *m/z* of adducted mass. σ was determined from one third of the difference between the empirical and theoretical, unadducted *m/z*. The adduct mass used for simulation of RPR in 6 mM Mg(OAc)$_2$ (Fig. S-2d) was obtained from the adducted mass of RPR observed in 4 mM Mg(OAc)$_2$ (Fig. S-2a). Since the adduct mass of RPR+POP5•RPP30 in 6 mM Mg(OAc)$_2$ was not available empirically for simulation, we used as reference the adduct mass observed in RPR+RPP21•RPP29 in 10 mM Mg(OAc)$_2$ (Table S-1).

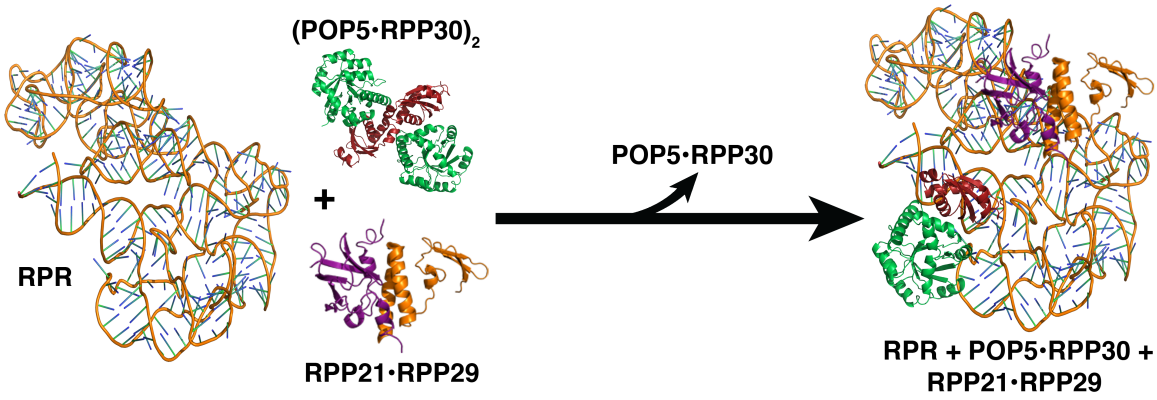

Figure S-3. Schematic illustrating assembly of *Pfu* RNase P based on results from our MS studies. The data show that RPP21•RPP29 exists as a heterodimer alone and in complex with the RPR, while POP5•RPP30 exists as a heterotetramer alone but assembles with the RPR as a heterodimer. Cartoons of the binary RPPs are from high-resolution structures,[8] while the model of *Pfu* RPR was generated based on homology with the crystal structure of the bacterial counterpart (Crowe, B. and Foster, M. P., unpublished).